

Temperature and final state effects in radio frequency spectroscopy experiments on atomic Fermi gases

Yan He, Chih-Chun Chien, Qijin Chen, and K. Levin

James Franck Institute and Department of Physics, University of Chicago, Chicago, Illinois 60637
(Dated: October 26, 2018)

We present a systematic characterization of the radio frequency (RF) spectra of homogeneous, paired atomic Fermi gases at finite temperatures, T , in the presence of final state interactions. The spectra, consisting of possible bound states and positive as well as negative detuning (ν) continua, satisfy exactly the zeroth- and first-moment sum rules at all T . We show how to detect the $\nu < 0$ continuum arising from thermally excited quasiparticles, which has not yet been seen experimentally. We explain semi-quantitatively recent RF experiments on “bound-bound” transitions and, thereby, predict the associated effects of varying temperature.

The superfluid and normal phases in trapped Fermi gases undergoing BCS to BEC crossover are presenting us with novel forms of superfluidity. An important characteristic of the superfluid is the pairing gap which is best probed using radio frequency (RF) spectroscopy [1, 2]. This technique has been applied experimentally in a trap integrated [1, 3] and tomographic [2] fashion. While early theoretical work [4, 5] addressed trap effects, more recently attention has been on final state effects [6, 7, 8, 9, 10] although, unfortunately, only at low or zero temperature. Many have viewed the importance of these experiments as a means of quantitatively measuring the ground state pairing gap, thereby testing different approaches to BCS-BEC crossover. Our point of view is that finite temperature is crucial to full experimental understanding as well as reliable assessments of theory.

The goal of this paper is to present a single formalism for the RF spectra at all frequencies and all T , including final state effects. A successful theory of a Fermi gas near unitarity, not only (i) has a pairing gap which appears [4, 5, 7] at $T^* > T_c$ but which, as T is decreased, (ii) exhibits a second order phase transition, at T_c . Studies of this smoothly varying (from above T^* to $T = 0$) pairing gap, reminiscent of its counterpart in the high T_c superconductors, may elucidate some of the physics of the cuprates [11]. On physical grounds [4, 5, 7] it is clear that the RF current $I(\nu)$ reflects the pairing gap $\Delta(T)$ rather than coherent superfluid order. At odds with this observation is the fact that all crossover theories which include pairing fluctuations [12, 13, 14, 15] except the present one, lead to first order transitions at T_c . In a related fashion, alternative calculations [8, 9, 16] of $I(\nu)$ consider only the low or zero T superfluid and/or separately the normal phase even though, at $T < T^*$, the presence or absence of superfluid order in the RF spectra should not lead to fundamentally different physics.

We consider a homogeneous system which is relevant to recent tomographic experiments [2] At $T \neq 0$, the spectrum consists of (possibly) bound state contributions which either appear at positive or negative detuning, ν and, (always), positive as well as negative ν continuum contributions which reflect the pairing gap, and can be used to measure its size. We emphasize the $\nu < 0$ continuum which derives from thermally excited quasiparticles has not yet been seen experimentally nor addressed theoretically. A central finding is that it can be strongly enhanced by final state interactions and made visi-

ble in future tomographic experiments. Near unitarity, final state effects make it possible to extract (using sum rules) the gap Δ as well as the chemical potential μ . We explain semi-quantitatively recent low T experiments and make predictions for the accompanying temperature dependences which should be observable.

The RF technique focuses on the three lowest energy atomic hyperfine states (two of which are involved in the pairing, while a third provides a final “excited” state for one component of a pair). For definiteness, we first consider a superfluid of pairs in the equally populated hyperfine 1-2 levels and apply a radio frequency ω_{23} to excite the atoms in state 2 to state 3, as described by a Hamiltonian given in Refs. [4, 5, 6, 7, 8, 9]. The RF response function can be obtained following the standard linear response theory [4, 5, 6]. Here we formulate the finite T , RF problem using a diagrammatic scheme which can be made compatible with the diagrams in Ref. 8, although attention in that paper was restricted to very low temperatures. We will see below that our diagrammatic scheme reduces at $T = 0$ to the approach of Ref. 9. This correspondence, and indeed, all diagrammatic formulations [7] of the RF experiments are based on a T -matrix approach. The T -matrix used here (for the 1-2 channel) is consistent [11, 17] with the BCS-Leggett ground state equations and involves one bare and one dressed Green’s function. We have

$$t_{12}^{-1}(Q) = g_{12}^{-1} + \sum_K G_1(K)G_2^0(Q - K) \quad (1)$$

$$t_{13}^{-1}(Q) = g_{13}^{-1} + \sum_K G_1(K)G_3^0(Q - K) \quad (2)$$

where we have introduced the dressed Green’s function $G = [(G^0)^{-1} - \Sigma]^{-1}$ and G^0 is the Green’s function of the non-interacting system. Here the subscripts indicate the hyperfine levels, $K \equiv (i\omega_l, \mathbf{k})$, $Q \equiv (i\Omega_n, \mathbf{q})$ are 4-momenta with $\sum_K \equiv T \sum_l \sum_{\mathbf{k}}$, etc., and ω_l and Ω_n are fermion and boson Matsubara frequencies, respectively. Throughout we take $\hbar = k_B = 1$ and assume a contact potential (so that the strict Hartree self-energy vanishes) and a (nearly) empty population in the hyperfine 3 state so that $G_3(K) \approx G_3^0(K)$. As has been demonstrated elsewhere [11], it is reasonable to take the self energy (on the real frequency axis) in the Green’s functions

G_1 and G_2 to be of the generalized BCS form

$$\Sigma(\omega, \mathbf{k}) \approx \frac{\Delta^2}{\omega + \epsilon_{\mathbf{k}}}, \quad (3)$$

although this approximation is not essential. Similarly, we have shown [11] that, below T_c , $\Delta(T)$ is constrained by a BCS-like gap equation which can be written as $1 + g_{12}\chi_{12}(0) = 0$ where $\chi_{12}(Q) = \sum_K G_1(K)G_2^0(Q-K)$, in conjunction with a fermion number equation. More generally, the propagator for noncondensed pairs is of the form $t_{12}(Q) = g_{12}/[1 + g_{12}\chi_{12}(Q)]$.

We emphasize a distinction between the pairing gap (which we call Δ) and the order parameter, called Δ_{sc} . The difference between these two energy scales can be shown [11] to be associated with noncondensed pair effects parameterized by the pseudogap Δ_{pg} defined by

$$\Delta_{pg}^2(T) = \Delta^2(T) - \Delta_{sc}^2(T). \quad (4)$$

Here we note that $\Delta_{pg}^2 = -\sum_{Q \neq 0} t_{12}(Q)$, which allows T_c to be determined [11] as the temperature where Δ_{sc} first vanishes. We find $T_c = 0.25T_F$ at unitarity. It is convenient notationally to define a form of Gor'kov F function in terms of the pairing gap as

$$\Delta G_2(K)G_1^0(-K) = \frac{\Delta}{\omega_l^2 + E_k^2} \equiv F(K),$$

where $E_k = \sqrt{\xi_k^2 + \Delta^2(T)}$, and $\xi_k = \epsilon_k - \mu$, $\epsilon_k = k^2/2m$. Because of the constraints imposed by the BCS-like gap equation, $t_{12}(Q)$ diverges at $Q = 0$ so that it is reasonable to set Q in t_{12} to zero, i.e., $t_{12}(Q) \approx -(\Delta^2/T)\delta(Q)$. This assumption, which leads to the simple form of Eq. (3), is not essential for understanding the physics but it does greatly simplify the calculations [18].

The resulting diagram set for the RF response function, $D(Q)$, is shown in Fig. 1 and this last approximation is equivalent to treating the Aslamazov-Larkin (AL) diagram (called D_{AL}) in Fig. 1 at the BCS mean-field level, leading to the opposite momenta $\pm K$ for particles 1 and 2 in the diagram. The leading order term, $D_0(Q)$, of the response function appears as the bubble on the left and was introduced in Ref. 4. The term on the right, $D_{AL}(Q)$, depends on Δ , not Δ_{sc} , and incorporates final-state effects via the interactions g_{12} between 1 and 2 and g_{13} between 1 and 3. We neglect the effects arising from the interaction between 2 and 3. This is consistent with the approach in Ref. 6. This second term has appeared previously in studies of the superfluid density [17].

Writing out the AL diagram yields

$$D_{AL}(Q) = \left[\sum_K F(K)G_3^0(K+Q) \right]^2 t_{13}(Q). \quad (5)$$

For the RF field, $Q = (i\Omega_n, \mathbf{0})$ so that $D(i\Omega_n) \equiv D(Q)$. We take μ_3 satisfying $f(\xi_{k,3}) = 0$, where $\xi_{k,3} = \epsilon_k - \mu_3$. Then the RF current, given by the retarded response function, is $I(\nu) \equiv -(1/\pi) \text{Im} D^R(\Omega)$, where $\Omega \equiv \nu + \mu - \mu_3$, and we find

$$D(Q) = D_0(Q) + \frac{[D_2(Q)]^2}{m/4\pi a_{13} + D_1(Q)}, \quad (6)$$

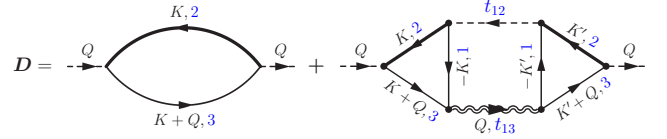


Figure 1: (Color online) Feynman diagrams for the RF response function $D(Q)$. The left bubble is the lowest order D_0 , whereas the right diagram, D_{AL} , is associated with final state effects. Here thin (thick) lines stand for bare (full) fermion propagators, the dashed line for t_{12} , approximated as the condensate, and double wiggly line for t_{13} . The numbers in blue indicate the hyperfine levels.

and $t_{13}^{-1}(Q) = m/4\pi a_{13} + D_1(Q)$, where a_{13} (and a_{12}) are the s -wave scattering length in the 1-3 (and 1-2) channels, respectively. Here $D_0(Q) = \sum_K G_2(K)G_3^0(K+Q)$

$$= \sum_K \left[\frac{f(E_k) - f(\xi_{k,3})}{i\Omega_n + E_k - \xi_{k,3}} u_k^2 + \frac{1 - f(\xi_{k,3}) - f(E_k)}{i\Omega_n - E_k - \xi_{k,3}} v_k^2 \right] \quad (7)$$

and $I_0(\nu) = -(1/\pi) \text{Im} D_0^R(\Omega)$. We also define $D_2(Q) \equiv \sum_K F(K)G_3^0(K+Q)$

$$= \sum_K \frac{\Delta}{2E_k} \left[\frac{1 - f(E_k) - f(\xi_{k,3})}{i\Omega_n - E_k - \xi_{k,3}} - \frac{f(E_k) - f(\xi_{k,3})}{i\Omega_n + E_k - \xi_{k,3}} \right] \quad (8)$$

and $D_1(Q) \equiv \sum_K G_1(K)G_3^0(Q-K) - \sum_{\mathbf{k}} (1/2\epsilon_{\mathbf{k}}) =$

$$\sum_K \left[\frac{f(E_k) + f(\xi_{k,3}) - 1}{i\Omega_n - E_k - \xi_{k,3}} u_k^2 + \frac{f(\xi_{k,3}) - f(E_k)}{i\Omega_n + E_k - \xi_{k,3}} v_k^2 \right] - \sum_{\mathbf{k}} \frac{m}{k^2}. \quad (9)$$

After analytical continuation and change of variables, we have $\Omega \pm E_{\mathbf{k}} - \xi_{k,3} = \nu \pm E_{\mathbf{k}} - \xi_{\mathbf{k}}$. Importantly, the denominators here are the same as those which appear in t_{12} . Furthermore, at $\nu = 0$, $f(\xi_{k,3})$ is cancelled out so that

$$t_{13}^{-1}(0) = (g_{13}^{-1} - g_{12}^{-1}) + t_{12}^{-1}(0) = g_{13}^{-1} - g_{12}^{-1}. \quad (10)$$

It follows that the complex functions $D_0(Q)$, $D_1(Q)$, and $D_2(Q)$ are the same as their wave function calculation counterparts [9] when the pairing gap Δ is chosen to be order parameter Δ_{sc} and $T = 0$. It is ν not Ω that should be identified with the experimental RF detuning.

After some straightforward algebra, one can show that when $g_{13} = g_{12}$ there is an exact cancellation such that $I(\nu) \sim \delta(\nu)$. In general, we have $I_0(\nu) = (1/\pi)(\Delta^2/\nu^2) \text{Im} \bar{t}_{13}^{-1,R}(\nu)$, and

$$I(\nu) = \left[\frac{1}{g_{12}} - \frac{1}{g_{13}} \right]^2 \frac{I_0(\nu)}{|\bar{t}_{13}^{-1,R}(\nu)|^2} = -\frac{1}{\pi} \left[\frac{m}{4\pi a_{13}} - \frac{m}{4\pi a_{12}} \right]^2 \frac{\Delta^2}{\nu^2} \text{Im} \bar{t}_{13}^R(\nu), \quad (11)$$

where $\bar{t}_{13}^R(\nu) \equiv t_{13}^R(\Omega)$.

Equations (11) are a central result of this paper which make it clear that final state effects in the RF current directly reflect the T -matrix in the 1-3 channel. In general, features in the RF

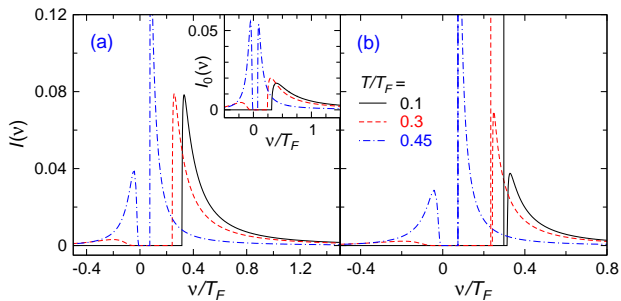


Figure 2: (Color online) RF current $I(\nu)$ as a function of RF detuning ν for transitions with unitarity $1/k_F a_{12} = 0$ at 834 G to final state (a) $1/k_F a_{13} = -1$ and (b) -0.5 in the BCS regime, corresponding to $T_F = 31$ and 124 kHz, respectively. The temperatures are $T/T_F = 0.1$ (Black solid), 0.3 (red dashed) and 0.45 (blue dot-dashed lines). Here $T_c = 0.25T_F$. The sharp lines next to the right continuum in (b) correspond to bound states. Inset: Lowest order RF current $I_0(\nu)$ vs ν .

spectra derive from the poles and imaginary parts of Eqs. (6)-(9). The spectrum may contain a bound state associated with poles at ν_0 in t_{13} , as determined by $t_{13}^{-1}(\nu_0) = 0$. This leads to the so called “bound-bound” transition. In addition, there is a continuum associated with both the numerator and denominator in the first of Eqs. (11), with each contribution spanned by the limits of $\nu = \xi_k \pm E_k$, i.e., $-(\sqrt{\mu^2 + \Delta^2} + \mu) \leq \nu \leq 0$ and $\nu \geq \sqrt{\mu^2 + \Delta^2} - \mu$. The continuum at positive frequencies is primarily associated with breaking a pair and promoting the state 2 to state 3. This represents the so-called “bound-free” transition. On the negative detuning side, the continuum is primarily associated with promoting to state 3 an already existing thermally excited 2 particle. The spectral weight of the negative continuum vanishes exponentially at low T as $e^{-\Delta/T}$. Therefore, there is a strong asymmetry in the continuum with the bulk of the weight on the positive frequency side for low T . If the bound state falls within the negative continuum, it will acquire a finite life time, and decay quickly at high T .

Of importance, in assessing a theoretical framework for computing the RF current are the two sum rules associated with the total integrated current and the first moment or “clock shift” [6]. Using the Kramers-Kronig relations between $\text{Re } t_{13}^R$ and $\text{Im } t_{13}^R$, it is easy to prove that, not only in the ground state, but also at finite temperature, Eq. (11) satisfies

$$\int d\nu I(\nu) = n_2 - n_3, \quad (12)$$

$$\int d\nu \nu I(\nu) = \Delta^2 \frac{m}{4\pi} \left(\frac{1}{a_{12}} - \frac{1}{a_{13}} \right), \quad (13)$$

where n_2 and $n_3 (= 0)$ are the density of state 2 and 3 atoms, respectively. In this way we find for the clock shift

$$\bar{\nu} = \frac{\int d\nu \nu I(\nu)}{\int d\nu I(\nu)} = \frac{\Delta^2}{n_2 - n_3} \frac{m}{4\pi} \left(\frac{1}{a_{12}} - \frac{1}{a_{13}} \right), \quad (14)$$

which agrees with Ref. [6] when $n_3 \rightarrow 0$. It should be stressed that this sum rule is satisfied only when $a_{13} \neq 0$ and when

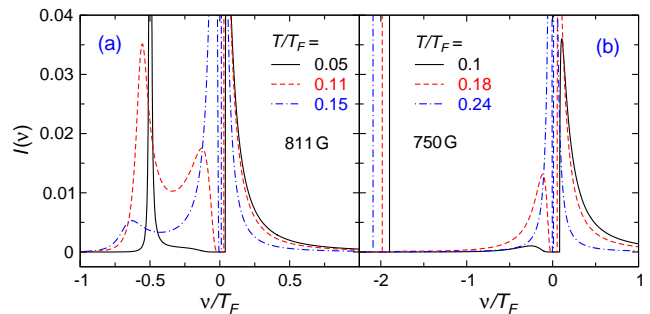


Figure 3: (Color online) RF current $I(\nu)$ as a function of detuning ν for $1 \rightarrow 2$ transitions in a 1-3 superfluid of $T_F = 40$ kHz (a) from $1/k_F a_{13} = -0.804$ to final states $1/k_F a_{23} = 0$ at 811 G, and (b) from $1/k_F a_{13} = -0.524$ to $1/k_F a_{23} = 0.68$ at 750 G, for different temperatures as labeled. Here $T_c/T_F = 0.15$ and 0.17, respectively. In (b) when T is high and Δ is small, the two peaks around $\nu = 0$ may not be resolvable experimentally.

both diagrammatic contributions are included. It is easy to show that at large ν , $I_0(\nu) \sim \nu^{-3/2}$, $\text{Im } t_{13}^R \sim \nu^{-1/2}$, so that $I(\nu) \sim \nu^{-5/2}$, in agreement with Ref. 8. Clearly, the first moment of $I(\nu)$ is integrable, whereas the first moment of $I_0(\nu)$ is not. Finally, Eq. (11) reveals that the spectral weight (including possible bound states) away from $\nu = 0$ will disappear when the gap Δ vanishes.

Figures 2(a) and 2(b) illustrate the behavior of the spectrum $I(\nu)$ when the initial state 1-2 pairing is at unitarity (i.e., at 834 G) and the final state 1-3 pairing is on the BCS side of the 1-3 resonance, for temperatures $T/T_F = 0.1, 0.3,$ and 0.45 . The parameters we use are taken from Ref. 19. The inset of Fig. 2(a) indicates the behavior in the absence of final state effects for the same temperatures. The asymmetry of the continuum around $\nu = 0$, discussed earlier, is evident even in this leading order bubble diagram. As T is raised the spectrum becomes more symmetric. In contrast to the findings in Ref. 16, and as consistent with experiments [1] on trapped gases, we do not find a substantial pairing gap at $T/T_F \approx 1$. In Fig. 2(a), the final state interaction $1/k_F a_{13} = -1$ is relatively weak, and there is no bound state. In contrast, at $1/k_F a_{13} = -0.5$ (or $T_F \approx 6\mu\text{K}$) in Fig. 2(b), a bound state emerges at low T (although it disappears at moderate temperatures when the gap becomes small). For the low $T_F \sim 2.5\mu\text{K}$ used in Ref. 1, we do not find a bound state. These results are consistent with $T = 0$ calculations of Basu and Mueller [9]. It should be stressed that, at 834 G for a typical T_F , when the bound-bound transition occurs, it is barely separated from the asymmetric bound-free continuum, which is always present.

Figure 3 presents the analogous plots at different T for RF transitions from an initial 1-3 superfluid with $T_F = 40$ kHz at (a) 811 and (b) 750 G, which are on the BCS side of the 1-3 resonance (which appears at 690 G). The system is subject to an RF field promoting state 1 to state 2. “Bound-bound-like transitions” [19] now appear. In Fig. 3(a), the bound state falls within the negative detuning continuum. Importantly, the disappearance of the bound state with temperature is preceded by a very unusual two-peaked spectrum in the negative detuning regime, which is seen at the two higher T . We can under-

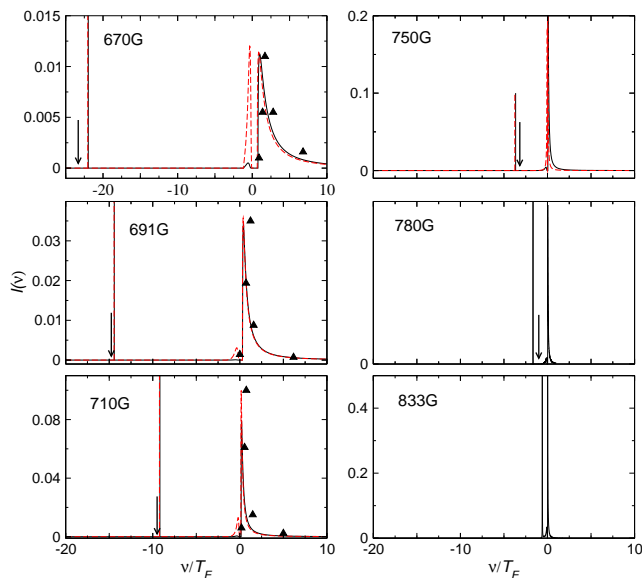


Figure 4: (Color online) RF current $I(\nu)$ as a function of detuning ν for a 1-3 superfluid with RF excitation from state 3 to state 2. The black curves are calculated at experimental parameters of $(1/k_F a_{13}, 1/k_F a_{12}, T/T_F) = (0.4, 3.3, 0.2), (0.0, 2.6, 0.1), (-0.3, 2.0, 0.1), (-0.7, 1.1, 0.09), (-0.9, 0.6, 0.09),$ and $(-1.2, 0.0, 0.06)$ from low to high fields. The red dashed curves are calculated at twice the temperatures. The sharp lines on the left indicate bound states. For comparison, experimental data are marked by arrows for bound peak locations and by triangles for the continuum. [20].

stand this unusual structure as a combination of the peak from the negative continuum which appears very close to $\nu = 0$, (as also seen in Figure 2) and the near-by bound state peak. At even higher T , the spectral weight will shift almost completely to the region near $\nu = 0^-$ and the bound state decays rapidly. As $\nu \rightarrow 0^-$, the negative continuum peak is a com-

bined effect of the vanishing $\text{Im} \bar{t}_{13}^R$ and the diverging factor $1/\nu^2$ in Eq. (11). In Fig. 3(b), the bound state is outside the continuum, and the binding energy is fairly insensitive to temperature. We have chosen experimentally accessible parameters here, so that the unusual double-peaked structure in $I(\nu)$ at $\nu < 0$ should be observable. Finally, we emphasize that the highest T cases in Figs. 2 and 3 are at or above T_c , so that the continuum appears only because there exists a pseudogap in the fermionic spectrum.

Figure 4 addresses recent data [2] associated with 1-3 pairing and RF excitation from state 3 to state 2. The calculations of $I(\nu)$ shown in the (black) solid curves in all six panels were performed with experimental parameters, and should be compared with Fig. 4 of Ref. [2]. To help in the comparison a number of data points (normalized to the same peak height) have been inserted. The sharp bound states will, in the data, be broadened both instrumentally and from limited spatial and energy resolution. Except for a slight broadening which we have ignored here, our calculated black solid curves, which incorporate final state effects, can be seen to be in semi-quantitative agreement with experiment. We anticipate that at higher T (red dashed lines), the negative ν continuum states should start to become apparent. Despite the presently good agreement, we feel the ultimate test of any theory must involve a test of its predictions, such as those shown here.

At unitarity, the best way to measure $\Delta(T)$ is using the sum rule in Eq. (14) and its experimental counterpart. Together with the $\nu > 0$ continuum threshold which appears at $\sqrt{\Delta^2 + \mu^2} - \mu$, one can also determine μ and hence the factor β . This analysis is possible only in the presence of final state effects. Because $I(\nu)$ at general T depends on the total pairing gap $\Delta(T)$, the size of the order parameter and pseudogap cannot be separately inferred (except when the order parameter vanishes above T_c).

This work is supported by Grants NSF PHY-0555325 and NSF-MRSEC DMR-0213745. We thank S. Basu, C. Chin, S. Jochim, and E. Mueller for helpful discussions.

-
- [1] C. Chin, M. Bartenstein, A. Altmeyer, S. Riedl, S. Jochim, J. H. Denschlag, and R. Grimm, *Science* **305**, 1128 (2004).
[2] C. Schunck, Y.-I. Shin, A. Schirotzek, and W. Ketterle, arXiv:0802.0341.
[3] C. H. Schunck, Y. Shin, A. Schirotzek, M. W. Zwierlein, and W. Ketterle, *Science* **316**, 867 (2007).
[4] J. Kinnunen, M. Rodriguez, and P. Törmä, *Science* **305**, 1131 (2004).
[5] Y. He, Q. J. Chen and K. Levin, *Phys. Rev. A* **72**, 011602(R) (2005); Y. He, C. C. Chien, Q. J. Chen and K. Levin, *Phys. Rev. A* **77**, 011602(R) (2008).
[6] Z. Yu and G. Baym, *Phys. Rev. A* **73**, 063601 (2006); G. Baym, C. J. Pethick, Z. Yu and M. W. Zwierlein, *Phys. Rev. Lett.* **99**, 190407 (2007).
[7] M. Punk and W. Zwerger, *Phys. Rev. Lett.* **99**, 170404 (2007).
[8] A. Perali, P. Pieri, and G. C. Strinati, *Phys. Rev. Lett.* **100**, 010402 (2008).
[9] S. Basu and E. Mueller, arXiv:0712.1007.
[10] M. J. Leskinen, V. Apaja, J. Kajala, and P. Törmä, arXiv:0802.1882.
[11] Q. J. Chen, J. Stajic, S. N. Tan, and K. Levin, *Phys. Rep.* **412**, 1 (2005).
[12] R. Haussmann, W. Rantner, S. Cerrito, and W. Zwerger, *Phys. Rev. A* **75**, 023610 (2007).
[13] P. Pieri, L. Pisani, and S. G. C, *Phys. Rev. B* **70**, 094508 (2004).
[14] N. Fukushima, Y. Ohashi, E. Taylor, and A. Griffin, *Phys. Rev. A* **75**, 033609 (2007).
[15] H. Hu, P. D. Drummond, and X. J. Liu, *Nat. Phys.* **3**, 469 (2007).
[16] P. Massignan, G. M. Bruun, and H. T. C. Stoof, *Phys. Rev. A* **77**, 031601(R) (2008).
[17] Q. J. Chen, I. Kosztin, B. Jankó, and K. Levin, *Phys. Rev. Lett.* **81**, 4708 (1998).
[18] Here we extend this approximation above the actual T_c as well, to estimate Δ and μ .
[19] C. Chin and P. S. Julienne, *Phys. Rev. A* **71**, 012713 (2005).
[20] Note that Ref. [2] has a different sign convention for ν .